J. Indian Inst. Sci., Mar.–Apr. 1989, **69**, 143–166

IISc THESES ABSTRACTS

Thesis Abstract (Ph.D.)

Electron spectroscopic studies of the adsorption and reactivity of oxygen on transition metal surfaces covered with alkali and alkaline earth metals by M. Ayyoob.
Research supervisor: M. S. Hegde.
Department: Solid State and Structural Chemistry.

1. Introduction

Alkali and alkaline earth metals are known to promote many catalytic reactions such as epoxidation and ammonia synthesis. Controversy still exists on the role of alkali metals in promoting Fisher-Tropsch reaction. The exact role of alkali and alkaline earth metals in altering surface properties of transition metals is not well understood although it has been a subject of study for several decades. It has now become possible to follow the changes in the surface properties of transition metals dosed with submonolayer coverages of alkali or alkaline earth metals under controlled experimental conditions employing surface analytical techniques. Before 1981 much of the studies on alkali-covered metal surfaces were essentially carried out employing thermal desorption spectroscopy (TDS), Auger electron spectroscopy (AES) and low-energy electron diffraction (LEED). X-ray photoelectron spectroscopy (XPS) is certainly a more powerful technique in identifying chemical state of surface adspecies from the chemical shifts. UV-photoelectron spectroscopy (UPS) is extremely useful in identifying atomic and molecular species from the valence band spectra. Quantitative estimations (within 5%) are possible in XPS from the intensities of core-level photoelectron spectra which can be used to follow surface reactions between the adspecies and the metal surface. Here, an attempt has been made to understand the role of alkali metals in altering the adsorption and reactivity of transition metal surfaces employing XPS, UPS and AES techniques with special emphasis on the adsorption of oxygen and its reactivity towards oxidation of CO, HCOOH, NH_3 and HCl.

2. Experimental

The adsorption studies on alkali-covered metal surfaces presented here have been carried out in UHV conditions using ESCA3 Mark II spectrometer of V.G. Scientific Ltd, UK equipped with facilities for MgKα and AlKα X-ray and UV-photoelectron spectroscopies and Auger electron spectroscopy. The alkali metals K and Cs were deposited by heating faujasite sources while barium was deposited from a getter source. XPS core level photolines have been extensively employed for accurate determination of surface concentrations of adspecies using photoionization cross sections and escape depths of the respective photoelectrons.

3. Results and discussion

The primary effect of alkali or alkaline earth metal dosed on a transition metal was found to be charge

transfer from alkali to the transition metal[1]. This was demonstrated by an increase in the occupancy of valence band of Cu on dosing barium, as inferred, for the first time, from an increase in the Cu(L_3VV)/Cu(L_3MM) Auger intensity ratio as a function of barium coverage. Increase in the Ni(L_3VV)/Ni(L_3MM) Auger ratio on barium coverage also showed charge transfer from Ba to Ni.

Oxygen adsorption and desorption studies on K-, Cs- or Ba-covered Cu, Ag, Au, Pt, Ni and Fe polycrystalline surfaces have been carried out employing XPS, UPS and AES techniques. Controlled experiments on the effect of surface concentrations of alkali metals (0.1 to 2.5×10^{15} atoms/cm^2) with different oxygen exposures (0.1 L to 10^4 LO_2) have been studied. Different types of oxygen species, *viz*., O^{2-} (528.5 to 530 eV), O^{1-} (530.5 to 531.5 eV) and $O_2^{\delta-}$ ($\delta \sim 2$; 532.5 to 533 eV) have been characterized by a careful examination of O(1s) region in XPS when oxygen is exposed to alkali-covered transition metal surfaces. Band positions of O^{1-} species around 10 and 12 eV, respectively, due to ^3P and ^1D states of O(ad) species have been assigned for the first time employing UPS[2]. On Cu covered with K or Ba, two types of oxygen species O^{2-}, O^{1-} were identified at 300K in contrast to a single O^{2-} species on clean Cu. O^{2-}, O^{1-} and $O_2^{\delta-}$ types of oxygen species are seen at 300 K when Ag is covered with K, Cs or Ba[3]. O^{1-} species are associated with alkali metal. On K- or B-covered Au surface, O^{1-} and $O_2^{\delta-}$ species are seen at 300 K. Intensity of molecularly chemisorbed $O_2^{\delta-}$ was higher at 80 K. Only O^{2-} and O^{1-} types of oxygen species associated with Pt and alkali metal, respectively, are observed on K- or Cs-covered Pt surface[3]. At lower barium coverages, Ni showed enhanced oxidation to NiO as compared with pure Ni while at coverages higher than 5×10^{14} Ba atoms/cm^2, oxidation of Ni was suppressed. Oxidation of Fe was suppressed at still higher barium coverages.

Quantitative estimations of surface concentrations of adspecies have been carried out in each of the above cases from the intensities of core-level photoelectron spectra. Saturated absolute surface concentrations of oxygen for a given alkali coverage and hence oxygen-to-alkali concentration ratio have been estimated over a wide range of alkali coverages as well as temperatures (300–800 K). The parameter, P_M, defined as the oxygen uptake coefficient at low alkali coverages $d\sigma_0/d\sigma_M$ as $\sigma_M \to 0$ has been determined for different metal-alkali systems[4]. For example, P_M varied as Ag/Ba > Ag/Cs > Ag/K for Ag surfaces with values 3.8, 3.1 and 2.5, respectively. XPS studies have also shown that desorption temperature of alkali metal increased in the presence of oxygen. Oxygen could be desorbed from Cu and Ni surfaces when covered with K or Ba (through a possible conversion of O^{2-} to O^{1-}) at temperatures lower than the dissociation temperatures of Cu_2O and NiO.

Coadsorption of oxygen and chlorine was studied on potassium- and barium-covered Ag surfaces to see if the intensity of molecular dioxygen species could be selectively enhanced or whether the O^{1-} and O^{2-} types of species could be selectively suppressed. This study has special relevance in the selective oxidation of ethylene on Ag catalysts[5]. XPS results indicated that surface O^{2-} and O^{1-} species were depleted on chlorination when chlorine was exposed to Ag covered with K or Ba saturated with oxygen. $O_2^{\delta-}$ was not affected. Also oxygen exposure on Ag + K or Ba surface predosed with chlorine showed only $O_2^{\delta-}$ species with O(1s)-binding energy at 533 eV Cl(ad) species associated with Ag are found to occupy a preferred site on the alkali-dosed surface involving chemisorptive replacement of O^{2-} to the subsurface region At lower potassium coverages, Cl(ad) was associated with Ag only whereas at higher potassium coverages, only KCl was observed as distinguished from Cl(2p) peaks. However, even at low barium coverages, two types of Cl(ad) species were observed, one associated with Ag and the other with barium.

X-ray UV photoelectron spectroscopic studies of the interaction of CO with oxygen on K-, Cs- and Ba-covered Ag surfaces showed the formation of carbonate at 300 K[6]. While on cesium-covered surface, only carbonate formation was observed, on the K- and Ba-covered surfaces, molecularly chemisorbed CO is also seen. The variation of the surface concentrations of carbon and oxygen with temperature was examined and a reaction sequence for the interaction of CO with adsorbed oxygen is

suggested. No adsorption of CO was seen on K- or Ba-covered Cu or Pt surfaces saturated with oxygen.

XPS and UPS studies on the adsorption of HCOOH on barium-covered Cu and Ag surfaces with oxygen showed an enhanced reactivity of O(ad) associated with Cu or Ag towards proton abstraction form HCOOH[7]. The formates associated with Cu or Ag showed greater thermal stability and higher activation energy of dissociation in the presence of barium. Decomposition of formate on oxygen-presorbed Cu showed only H_2O and CO_2, but on the barium-covered Cu surface, the formation of CO was also observed. Decomposition pathways of the HCOO(ad) species on the barium-dosed Cu and Ag surfaces have been suggested.

Oxidation of NH_3 has been studied on clean and potassium-covered Pt surfaces employing XPS technique[8]. On the clean Pt surface exposed to oxygen, the reaction $NH_3 + O(ad) \rightarrow H_2O + NH$ occurred with the complete removal of adsorbed oxygen in the formation of H_2O. But on the potassium-covered Pt surface saturated with oxygen, surface concentration of oxygen was much higher and the total oxidation reaction $NH_3 + O(ad) \rightarrow NO + H_2O$ was clearly seen even at 85 K.

Effect of alkali on the oxidation and reactivity of a typical nontransition metal, *viz.*, Pb, was also studied employing XPS and UPS techniques[9,10]. At lower barium coverages, more of PbO was formed compared to that on $Pb + O_2$ at 300 K. Proton abstraction from HCl occurred on oxidized Pb leading to $PbCl_2 + H_2O$ but on excess HCl exposure at 300 K, evaporation of $Pb(HCl_2)_2$ occurred leaving the Pb surface clean. But on the Ba-covered Pb surface, the activation energy of the novel reaction $PbCl_2 + 2HCl \rightarrow Pb(HCl_2)_2$ was increased due to electronic effects and not due to subsurface oxygen as was believed earlier[11]. Thus, the alkali-promoted metal surfaces showed good potential for selective surface modification and/or stabilization of surface oxygen species which in turn proved fruitful in enhancing or modifying oxidation reaction pathways. XPS, UPS and AES have been proved to be extremely useful in such studies.

References

1. AYYOOB, M AND HEGDE, M. S. Adsorption of oxygen on clean and barium covered Cu surfaces: An XPS, UPS and AES study, *Surface Sci.*, 1984, **147**, 361–376.
2. HEGDE, M. S. AND AYYOOB, M O^{2-} and O^{1-} types of oxygen species on Ni and barium dosed Ni and Cu surfaces, *Surface Sci. Lett.*, 1986, **173**, L635–L640
3. AYYOOB, M. AND HEGDE, M. S. An XPS study of the adsorption of oxygen on Ag and Pt surfaces covered with K or Cs, *Surface Sci.*, 1983, **133**, 561–532.
4. HEGDE, M S. AND AYYOOB, M. Surface chemistry of alkali covered metals, *Proc. Indian Natn. Sci. Acad.*, 1985, **51A**, 256–285.
5. AYYOOB, M. AND HEGDE, M. S. Chlorination of Ag dosed with K or Ba in presence of oxygen: An XPS study, *J. Catalysis*, 1986, **97**, 516–526.
6. AYYOOB, M. AND HEGDE, M. S. X-ray and U.V. photoelectron spectroscopy studies of the interaction of CO with oxygen adsorbed on Ag covered with K, Cs or Ba, *J. Chem. Soc., Faraday Trans. I*, 1984, **80**, 2703–2713.
7. AYYOOB, M. AND HEGDE, M. S. Electron spectroscopic studies of formic acid adsorption and oxidation on Cu and Ag dosed with Ba, *J. Chem Soc., Faraday Trans I*, 1986, **82**, 1651–1662.
8. AYYOOB, M. AND HEGDE, M. S. An XPS study of the oxidation of NH_3 on K-covered Pt surface, *Indian J. Chem.*, 1983, **22A**, 465–468.

9. CARLEY, A. F., HEGDE, M. S. AND ROBERTS, M. W. A novel reaction at a Pb(110) surface, *Chem. Phys. Lett.*, 1982, **90**, 108–110.

10. AYYOOB, M. Electron spectroscopic studies of adsorption and reactivity of oxygen on alkali dosed metals, *Proc. Solid St. Phys. Symp.*, Pantnagar, 1986, **29C**, 29.

11. AYYOOB, M. AND HEGDE, M. S. Adsorption and reactivity of oxygen on barium promoted lead surface, *J. Chem. Soc., Faraday Trans. I*, 1988, **84**, 2377–2386.

Thesis Abstract (Ph.D.)

Physico-chemical studies on soils of the tea-growing areas in Southern India by S. Natesan.
Research supervisors: V. Krishnan and V. Ranganathan.
Department: Inorganic and Physical Chemistry.

1. Introduction

Soil is a complex and dynamic system. The physico-chemical studies on soils are important in understanding the fundamental soil characteristics[1]. These are useful in the formulation of fertilizer management and agronomic practices in crop cultivation, especially of tea in the present context[2]. The studies reported in this thesis are directed towards the soils in the tea-growing areas in Southern India, with a view to develop a comprehensive understanding of several soil properties, *viz.*, general physico-chemical characteristics, mineralogy of sand and clay, charge characteristics, water-retention characteristics and electro-ultrafiltration analysis of soils. In addition, the thesis discusses the results, utilizing different statistical techniques wherever necessary, for better understanding of chemistry of acid soils, in general, and particularly the relationships among various soil characteristics, and for suggesting utility of the information in soil and fertilizer management and agronomic practices for efficient crop production.

2. Experimental programme

Sixteen soil samples, collected from carefully chosen sites at different geographical locations representing the different tea-growing regions in Southern India, are utilized for the investigation. The physico-chemical properties of the soils include particle-size distribution, selected physical and chemical properties, forms of K^+, phosphorus fractions, mineralogy of sand and clay fraction, surface charge, water-retention characteristics and important available nutrients. These aspects are investigated using diverse techniques, *viz.*, chemical analysis, X-ray powder diffraction method, thermal analysis, petrographic examination, potentiometric titration, ion-adsorption measurement, moisture-retention study and electro-ultrafiltration (EUF) method. Statistical methods are employed, wherever necessary, for fitting the data and interpretation of results.

3. Main results and conclusions

The soils are found to be highly acidic and the acidity is associated with high-exchangeable Al^{3+} and low-exchangeable bases (Ca^{2+} and Mg^{2+}). The cation exchange capacity (CEC) of the soils is found to be low while the proportion of variable charge is high. All the soils possess a net negative surface charge at the existing soil pH conditions. Investigations on various chemical parameters show similarity in the nature of soils although their physical and chemical properties

Table 1
Selected characteristics of soils in the tea-growing regions of Southern India

Character	Mean (Range)/Relative order/Remarks
A. *General*	
pH (H_2O)	4.93 (3.93 to 6.53)
pH (KCl)	4.15 (3.68 to 5.35)
Organic carbon (%)	2.18 (0.97 to 4.64)
[a]Exchangeable Al^{3+}	2.71 (0.03 to 7.12)
[a]Σ bases	4.56 (1.63 to 10.41)
[a]Exchange acidity	21.18 (8.14 to 41.21)
[a]Effective CEC	7.27 (2.87 to 12.58)
[a]Variable charge	18.47 (8.11 to 34.42)
Variable charge ratio	0.71 (0.44 to 0.78)
B. *Mineralogy of fine sand and clay*	
(i) Fine sand	
Light minerals	Quartz ≫ Feldspar > Sericite > Perthite
Heavy minerals	Magnetite ≫ Ilmenite > Biotite
(ii) Clay	Kaolinite > Chlorite > Mica Gibbsite > Interstratified minerals
C. *Charge*	
[a]CEC at pH 4.8	8.53 (3.75 to 16.16)
[a]CEC at pH 7.0	14.53 (6.07 to 27.87)
[a]CEC at pH 8.2	16.64 (7.23 to 30.73)
$\pm pH(pH_{KCl} - pH_{H_2O})$	−0.78 (−0.25 to −1.18)
pH_0	3.6 to 4.2
[a]σ_p (permanent charge)	0.4 to 2.50
D. *Water-retention*	
Strongest direct effect on m, θ, and A_w	Bulk density, clay content and bulk density
Least direct effect on m, θ, and A_w	Organic carbon
Indirect effect on m, θ, and A_w	Organic matter *via* bulk density and pore space
E. *EUF analysis*	
Relationship between EUF and conventional soil test methods	Good

[a]unit in c mol(±) kg^{-1}

vary from one geographical location to another. Low-silt content, highly acidic nature, fairly large amounts of sesquioxides, low CEC and exchangeable bases, forms of K^+, and phosphate fractions provide useful information and suggest that the soils in this region of humid tropical to sub-tropical climatic conditions have undergone fairly intense weathering.

Mineralogical investigations of fine sand and clay fraction reveal that (a) quartz is the dominant mineral followed by feldspars, sericite and perthite in the light fraction, while opaques are the dominant minerals followed by ferromagnesium minerals (biotite, pyroxene and amphibole) in the heavy fraction of fine sand, and (b) kaolinite followed by chlorite are the dominant clay minerals, with appreciable amounts of gibbsite, illitic mica and interstratified(mica-chlorite) minerals. It is observed that the altitude and rainfall in the different locations influence the occurrence of certain clay minerals.

Soils at low-altitude and high-rainfall areas have kaolinite as the predominant clay mineral, while those at high-altitude and low-rainfall areas have relatively high amounts of chlorite dominant 2:1 phyllosilicates. Formation of gibbsite is favoured at high than at low-rainfall areas.

In view of the fact that most soil properties are dependent upon processes occurring at the surfaces of soil particles, the charge characteristics, *viz.*, the constant and variable surface charge of the soils has been investigated. It is revealed that the soils behave predominantly as variable surface charge colloid, and possess both positive and negative surface charges. The magnitude of the negative charge that develops at high pH is much larger than that of positive charge at low pH. One of the most important findings of the charge characteristics of the soils is that the pH_0 of the soils is lower than the soil pH, and the permanent charge is negative and small in magnitude. The point of zero net charge (PZNC) of the soils is found to be lower than pH_0 and is influenced by ionic strength of the supporting electrolyte. The implications of the charge characteristics for soil management practices pertaining to tea are discussed. Organic matter, specifically adsorbing ions like phosphate and silicate, reduces the pH_0, thus making the net surface charge more negative.

Water-retention characteristics of the soils are studied for resolving the effect of physico-chemical properties on the constants, *viz.*, m, θ_1 and A_ω, of water-retention characteristics. The path-coefficient analysis helps to resolve the direct and indirect effects of physico-chemical properties on m, θ_1 and A_ω. It is found that bulk density has the strongest direct effect on m and A_ω, while both the clay content and the bulk density have more or less equal direct effect on θ_1. The organic carbon content is found to have the least direct effect on all the three, *viz.*, m, θ_1 and A_ω, parameters. However, the indirect effect of organic matter, *via* bulk density and pore space is found to be quite appreciable. The organic matter is found to hold much of the water stored in it in the tension range above wilting. The results, further, reveal the possibility of simulating soil-moisture characteristic from easily determinable physico-chemical properties.

The EUF method of soil analysis has been explored in the present study to assess the EUF-extractable nutrients, and their relationships with conventional soil test-extractable nutrients[1]. It is found that there exist close relationships of EUF–N, EUF–P and EUF–K with conventional soil test-extractable N, P and K values, respectively. We have observed that EUF–N and EUF–P, extractable at 20°C, are significantly associated with tea productivity. Further, we are able to provide evidence for the low K^+ reserves in the soils from the EUF–K at 80°C and the ratio of EUF–K at 80°C to EUF–K at 20°C.

The results of the investigations have a direct bearing on the fertilizer management and agronomic practices pertaining to tea cultivation.

References

1 GREENLAND, D. J. AND HAYES, M. H. B. (ED.) *The chemistry of soil processes*, Wiley, 1981.

2 RANGANATHAN, V. AND NATESAN, S. Potassium nutrition of tea. In *Potassium in agriculture*, (ed.) R. D. Munson, ASA, CSSA, SSSA, Madison, Wisconsin, U.S.A., 1985, 981–1022.

3 NATESAN, S., RANGANATHAN, V., NEMETH, K. AND KRISHNAN, V. EUF-analysis of tea soils of Southern India and tea productivity, *Pl. Soil*, 1985, **83**, 191–198.

Thesis Abstract (Ph.D.)

X-ray structural studies on metal complexes of vitamin B_6-related compounds
by S. P. Sudhakara Rao.
Research supervisor: H. Manohar.
Department: Inorganic and Physical Chemistry.

This thesis embodies the syntheses, characterization and structural studies on metal complexes of vitamin B_6-related compounds. Spectroscopic techniques have been used to characterize the compounds and X-ray crystallography has been the main tool for the structure determination.

Among the vitamin B_6 constitutents, pyridoxal (PL) or pyridoxal phosphate (PLP) are important coenzymes responsible for many enzymatic reactions involving amino-acid metabolism such as transamination, racemization, decarboxylation, etc[1,2]. Ever since the discovery of the catalytic role of metal ions in nonenzymatic model reactions by Snell and coworkers[3], the study on the interactions of metal ions with vitamin B_6 constituents or with pyridoxylidene-amino acid Schiff bases has gained immense interest[4-6]. The present investigations by the author are concerned with the syntheses and structural characterization of: (i) metal complexes of pyridoxylidene Schiff bases, and (ii) ternary metal complexes of vitamin B_6 constituents or derivatives with 2, 2′-bipyridyl (BP). The details of the work done are presented in five chapters.

Chapter I, which serves as a brief introduction to the field, contains a general review on the various reaction types of PL-catalyzed processes in nonenzymatic systems and the role of metal ions in such processes. Brief mention is made of the X-ray studies of vitamin B_6 components as well as their metal complexes.

Preparation and spectroscopic characterization of five metal-Schiff base complexes, $Ni(PLNH)_2 \cdot 6H_2O$, $Ni(PL_2en) \cdot 3H_2O$, $Cu(PL_2en) \cdot 3H_2O$, $Ni(PLgly)_2 \cdot 6H_2O$ and $Cu(PLPgly) \cdot 4H_2O$ (PLNH = pyridoxylideneimine; PL_2en = N, N′-ethylenebis (pyridoxylideneimine), PLgly = pyridoxylideneglycine and PLPgly = 5′-phosphopyridoxylideneglycine) are covered in Chapter II. The bidentate PLNH and the tetradentate PL_2en ligands provide a square planar arrangement around the metal ion in their complexes. The remaining two ligands are tridentate. In the case of $Cu(PLPgly) \cdot 4H_2O$, studies have indicated the coordination from water and phosphate oxygens suggesting a distorted octahedral or square pyramidal structure for the complex.

Chapter III describes X-ray structural studies on two Schiff base complexes, $[Cu(PLPgly)(H_2O)] \cdot 3H_2O$ and $[Ni(PLgly)_2] \cdot 6H_2O$ The structures were solved by heavy atom method and refined by least-square procedures to values of 0.064 and 0.129 for 1464 and 1857 reflections, respectively. In $[Ni(PLgly)_2] \cdot 6H_2O$, the central metal ion has an octahedral environment with phenolic O, imine N and carboxylate O as the donor sites from each of the tridentate Schiff base ligands. However, in $[Cu(PLPgly)(H_2O)] \cdot 3H_2O$, the coordination geometry is square pyramidal with the three donors of the Schiff base and a water molecule forming the base and a phosphate O of a neighbouring molecule forming the axial site of the square pyramid. The interesting observation made in these structures is that the ligand is nearly planar in the Cu complex while it is very much off planarity in the Ni complex. Attempts are made to correlate the differences in the reactivities of Cu(II) and Ni(II) chelates to the differences in the stereochemistries of the respective chelates.

Though a few solution studies are done on ternary vitamin B_6 complexes[7], there appears to be no crystallographic studies on such systems. The preparation of two ternary complexes of the formulae $[Co(BP)_2(PN\text{-}H)] (ClO_4)_2$ and $[Cu(BP)(PN)Cl]ClO_4 \cdot H_2O$ (BP = 2, 2′- bipyridine, PN = neutral pyridoxine, PN-H = anionic pyridoxine) and their X-ray structure determination have

been described in Chapter IV. The structures were solved by heavy atom method and refined by full-matrix least-square procedures to R values of 0.080 and 0.042 for 3401 and 2094 reflections, respectively. Co(III) has an octahedral environment whereas Cu(II) has a square pyramidal geometry. Phenolic O and 4-(hydroxymethyl) O of both PN and PN-H and two Ns of the BP are the coordination sites in the complexes. Axial site in the Cu complex has been filled by a chloride ion. In both the complexes, PN or PN-H exists as a tautomer wherein phenolic O is deprotonated and pyridine N is protonated. However, in the Co complex the interesting feature observed is that the vitamin B_6 constituent exists as a new anionic species, PN-H, where the 4-(hydroxymethyl) group is deprotonated due to coordination to highly acidic Co(III).

Attempts to prepare ternary metal complexes of pyridoxylideneamino-acid Schiff bases culminated in the oxidation of pyridoxal to pyridoxic acid (PA) or its lactone (PAL) and their complex formation. Chapter V describes X-ray structures of three such compounds, (1) Cu(BP)(PA)Cl.2H_2O, (2) Cu(BP)(PA)(ClO_4), and (3) Cu(BP)(PAL)(NO_3) NO_3. These are the first examples of complexes containing PA and PAL. The structures were refined to R values of 0.079, 0.039 and 0.049 for 1807, 1624 and 3054 reflections, respectively. White phenolic O has been one of the donor sites as usual, the second one is carboxylate O in PA and carbonyl O in PAL. The coordination geometry around the metal ion is distorted square pyramidal in (1) and (3), and tetragonally elongated (4 + 1 + 1) octahedral in (2). Two sites each from PA or PAL and BP form the base of the square pyramid or octahedron and the axial site is either Cl, perchlorate O, or nitrate O. The phenolic O in (2) exhibits unusual nature in that it bridges two metal centres with unsymmetrical metal-donor distances, thus making the molecule a dimer: A possible mechanism for the oxidation of pyridoxal involving Cu(II)-BP moiety *via* Cu(I) intermediate has been detailed towards the end of the chapter.

The appendix deals with the crystal structure analysis of pyridoxal-free base. The structure was solved by direct method and refined to an R value of 0.040 for 897 reflections. The molecules exist in hemiacetal form and are stacked in a *trans* fashion.

References

1. HOLM, R. H — in *Inorganic biochemistry*, (ed.) G. L. Eichhorn, Elsevier, 1973, Vol. 2, pp 1137–1167.
2. MARTELL, A. E. — *Adv. Enzymol. Related Areas Mol Biol.*, 1982, **53**, 163.
3. LONGENECKER, J. B. AND SNELL, E. E. — *J. Am. Chem. Soc.*, 1957, **79**, 142–145.
4. METZLER, D. E. — *Adv. Enzymol. Related Areas Mol. Biol.*, 1979, **50**, 1.
5. VEDERAS, J. C. AND FLOSS, H. G. — *Acc. Chem. Res.*, 1980, **13**, 455, and references therein.
6. MARTELL, A. E. AND TAYLOR, P. — *Inorg. Chem.*, 1984, **23**, 2734–2735.
7. MARAFIE, H. M., EL-EZABY, M. S., RASHAD, M. AND NAGUIB, M. M — *Polyhedron*, 1984, **3**, 787–797 and references therein.

Thesis Abstract (Ph.D.)

The mechanism of the oxidative degradation, ignition and combustion of polystyrene in the presence of transition metal salicylates by R. Nagarajan.
Research supervisor: K. Kishore.
Department: Inorganic and Physical Chemistry.

1. Introduction

The extensive use, for various reasons, of catalysts during polymerization has led to metal ion impurities in commercial polymers. A detailed study of the combustion of polymers in the presence of metal ions will therefore be useful in fire research and flame retardancy. Hence, in the present investigations it was decided to study the mechanism of the metal-catalysed oxidative degradation, ignition and combustion of polystyrene (PS), which is one of the most widely used polymers. Fe, Co, Mn and Ni salicylates were used as the additives and their effect in the above mentioned phenomena was studied in detail.

2. Experimental

Thermal analysis techniques such as TGA and DTA were employed for the studies. In addition, apparatus was designed in the lab for specific experiments, such as ignition delay. Spectroscopic and chromatographic techniques were also employed wherever appropriate *e.g.*, IR, UV and HPLC.

3. Major results and discussion

From the present investigations it was possible to propose a mechanism for the thermal decomposition of the salicylates in air. It was found that the salicylates undergo a three-step decomposition—the first step involves the loss of water of crystallization, the second removal of one of the salicylate moeties and the third the oxidation of the residue to oxide.

The effect of the additives on the oxidative degradation, ignition and combustion of PS was studied in detail. It was found that the salicylates sensitize all the three phenomena. From detailed studies, it was found that the existing mechanism proposed for the metal catalysis at low temperatures was not operative at high temperatures. It has been established in the present studies that the metal ions exert their activity by interacting in the propagation step. A mechanism has been proposed giving the probable reactions that can take place during propagation which enhance the overall rate of degradation in the presence of the metal ions.

In the present studies an attempt has been made to predict the burning rates of polymers by employing the concept of 'mean fragment size' (MFS) developed in our laboratory. An already existing equation[1] which has employed the concept of 'critical fragment size' (CFS) was modified using MFS and numerically integrated to arrive at the burning rate. It was found that the predicted burning rates matched with the experimentally measured ones for PS.

The effect of the additives on the decomposition, ignition and combustion was also studied and it was found that the additives sensitize these phenomena in propellants also. Based on solid-phase thermal model the effect of these salicylates has been explained. It has been shown that the solid-phase thermal model is applicable when the heat released in the condensed phase is considerable.

Reference

1. RABINOVITCH, B. *Symp. (Int.) Comb. (Proc.)*, 1964, **10**, 1935.

Thesis Abstract (Ph.D.)

Studies on the structure and flammability of aromatic polyphosphates: a correlative approach by K. S. Annakutty.
Research supervisor: K. Kishore.
Department: Inorganic and Physical Chemistry.

1. Introduction

Polyphosphate esters are an important class of organophosphorus polymers in that, in addition to their flame-retardant characteristics as in the case of other organophosphorus polymers, they possess attractive plasticising properties too. Much attention has been drawn towards polyphosphates, mainly as polymeric additives to other polymers; the polymeric additives are preferred to conventional non-polymeric ones due to their better resistance to extraction, migration, volatile-loss, etc., thus making the flame retardancy to be available permanently. The literature on polyphosphates, notwithstanding a large number of patents, does not provide any systematic studies on the synthesis and thermal or flammability properties of these polymers. This type of a study would, in fact, throw much light on the mechanism of their flame-retardant action.

2. Experimental

Spectroscopic techniques like IR, ^{1}H, ^{13}C and ^{31}P NMR were used for the characterization of the polymers and thermal analysis techniques like TG and DTA were employed for the studies. In addition, apparatus was designed in the lab for the evaluation of flammability such as limiting oxygen index (LOI), ignition delay and mass burning rate. Pyrolysis gas chromatography was used to study the thermal degradation products of the polyphosphates.

3. Results and discussion

In the present investigation, a number of aromatic phosphate polymers with different chemical structures have been synthesized. The polymers were characterized by IR and ^{1}H, ^{13}C and ^{31}P NMR spectroscopy. Thermal stability and flammabilty of the polyphosphates were evaluated by thermogravimetry and LOI, respectively. The conventional correlation of char percentage with the LOI values was found to be unsatisfactory in the case of polyphosphates. However, it was found that the flammability of the phosphate polymers is a combined effect of thermal stability and phosphorus content. An empirical relationship existing among these three parameters has been derived considering a total of 13 polymers.

Phosphorus-based flame retardants are well-known for their condensed phase mechanism of flame-retardant action. However, the analysis of the thermal degradation products of polyphosphates by pyrolysis gas chromatography showed the presence of phosphate compounds in the gaseous phase. This observation coupled with the poor correlation between the char percentage and LOI undoubtedly supports the existence of a gaseous phase mechanism for polyphosphates. The fact that condensed

phase mechanism is also operative in polyphosphates is supported by the identification of phosphoric acid in the char; phosphoric acid is well-known for its action in the condensed phase through char formation.

These polyphosphates were successfully tried as polymeric flame-retardant plasticizers in polyvinyl chloride (PVC) for the first time. It has been generally observed that simple additives, though suppress combustion, sensitize ignition. However, the polymeric additives (polyphosphates), when added even in small quantities like 10% to a composition containing 50% PVC and 40% dibutyl phthalate, were found to suppress both combustion and ignition. Flame-retardant additives which suppress both combustion and ignition of polymers are hitherto unknown.

References

1. Petreus, O., Popescu, N. F., Rosescu, L., Delfin, C. G. and Ciolcă, D. *Rom. Pat.*, 1984, **84**, 115.

2. Van Krevelen, D. W. *Polymer*, 1975, **16**, 615–620.

Thesis Abstract (Ph.D.)

Studies on the regulation of chorionic gonadotropin in primate placenta by N. Mathialagan.
Research supervisor: A. Jagannadha Rao.
Department: Biochemistry.

1. Introduction

It is now very well established that the hypothalamus elaborates a number of releasing factors which regulates the function of pituitary. The secretion of pituitary gonadotropins, LH and FSH, is regulated by GnRH, a decapeptide, of hypothalamic origin[1]. During the last few years the presence of GnRH in different tissues other than hypothalamus has been demonstrated[2,3]. Takagi[4] and Gibbons *et al*[5] were the first to demonstrate the presence of GnRH- and TRH-like materials in human placenta and subsequently several reports have appeared on the presence of extrahypothalamic GnRH. These studies have revealed that the placental GnRH is very similar to hypothalamic GnRH. Khodr *et al*[6] suggested a possible role for the placental GnRH in the regulation of CG secretion by the placenta. In view of these observations, and the fact that the presence of functional and structural similarity between CG and LH and the regulation of pituitary LH by hypothalamic GnRH, it is not completely unjustified to expect that the placental CG secretion may also be subject to regulation by placental GnRH. The first trimester human placental minces and early pregnancy monkey placental minces were used to study the effect of GnRH addition on CG secretion *in vitro*.

2. Experimental procedure

Radioimmunoassays were standardised to quantitate human CG, monkey C, progesterone and estradiol-17β. A solid-phase radioimmunoassay (RIA) was developed using epoxy-activated cellulose as solid matrix in order to reduce the assay duration.

An *in vitro* experimental system utilising the first trimester human placental minces was standardised. This consisted of incubating the placental minces at 37°C under 95 O_2 and 5 CO_2 for different time

intervals with or without GnRH analogues. This system has been validated by monitoring the incorporation of ^{3}H-thymidine into DNA, ^{14}C-chlorella protein hydrolysate into protein and immunoprecipitation of labelled hCG using specific hCG antiserum. Similar experimental conditions were employed to study the effect of GnRH and Buserelin on mCG release from the bonnet monkey placental minces *in vitro*.

3. Results and discussion

It has been shown that addition of low concentration of GnRH or its agonists (D-Phe^{6}-GnRH, Buserelin)caused a significant increase in CG in medium while high concentration caused an inhibition suggesting a differential regulation as in the case of pituitary system. Using the monkey placental mince system, it was demonstrated that synthetic GnRH and its analogues exhibited a similar response on the hCG secretion into the medium. Studies carried out using ^{35}S-methionine and ^{3}H-glucosamine to monitor the synthesis of hCG revealed that addition of GnRH caused a significant increase in the immunoprecipitable hCG. These results suggested that GnRH stimulates both secretion as well as synthesis of CG in placenta.

The first event in the action of any hormone is the binding of the hormone to the specific receptor in the target site. In view of this it was of interest to examine whether there are any specific binding sites for GnRH in first trimester human placenta. The presence of binding sites for GnRH in the membrane fractions of the first trimester human placenta was identified and were found to have low affinity.

Calcium acts as a second messenger in mediating the GnRH-stimulated LH secretion from pituitary. Studies were carried out in the presence and absence of specific Ca^{2+} chelators EDTA and EGTA and also using $^{45}Ca^{2+}$ as a probe to monitor the influx and efflux of Ca^{2+} following GnRH addition. These studies revealed that following calcium depletion, there was significant decrease in the immunoassayable CG in the medium. Furthermore, addition of GnRH to first trimester human placental minces resulted in a dose-dependent $^{45}Ca^{2+}$ uptake and a concomitant increase in immunoreactive hCG secreted into the medium. Also following preincubation of placental minces with $^{45}Ca^{2+}$ and addition of GnRH, there was a rapid decrease in tissue of $^{45}Ca^{2+}$ within two minutes indicating that mobilisation and secretion of hCG are interrelated events.

A sensitive RIA for GnRH was developed and validated. Using the GnRH RIA, the presence and biosynthesis of GNRH like molecular in the first trimester human placenta was shown.

The placental GnRH has been characterized by carboxy methyl cellulose chromatography, high-pressure gel permeation chromatography, reverse-phase chromatography and finally establishing its biological activity *in vitro* by rat pituitary LH release assay.

In addition to the above *in vitro* demonstration, we have shown that the intravenous injection of 100 ug of GnRH proethylamide causes a rapid increase in the serum hCG in monkeys during early pregnancy[7]. Thus both *in vitro* and *in vivo* experimental results clearly establish that placental GnRH has an important role in the regulation of CG secretion. It will be of interest to examine whether a mechanism similar to that of hypothalamus wherein gonadal steroids regulate GnRH levels is also operative in the placenta.

References

1. JUTISZ, M. Gonadoliberin, in *Hormonal protamins and peptides* (Li, C. H. (ed.)), Vol. 7, pp. 98, Academic Press, 1979.

2	HEDGER, M P., ROBERTSON, D. M., BROWNE, C. A. AND DE KRESTER, D M.	*Mol Cell. Endocr.*, 1985, **42**, 163–174.
3.	GAUTRON, J P., PATTOU, E. AND KORDON, C	*Mol. Cell. Endocr.*, 1981, **24**, 1–15.
4.	TAKAGI, S.	*Nippon Samka – Fukinka Gakkai Zasshi*, 1971, **23**, 750.
5.	GIBBONS, J M. JR., MITNICK, M AND CHIEFFO, V.	*Am J Obstet. Gynecol*, 1975, **121**, 127.
6.	KHODR, G S AND SHER-KHODR, T. M	*Fertil. Steril.*, 1978, **30**, 301.
7.	RAO, A. J., MATHIALAGAN, N., KOTAGI, S. G. AND MOUDGAL, N. R.	*J. Biosci.*, 1984, **6** (Suppl. 2), 99.

Thesis Abstract (Ph.D.)

Mevalonate metabolism in plants by R. Lalitha.
Research supervisor: T. Ramasarma.
Department: Biochemistry.

1. Introduction

Plants produce a variety of isoprenoid products which include sterols, polyterpenes, polyprenols, essential oils and the plant growth regulators, abscisic and gibberellic acids. Although extensive work has been done on the identification of these compounds in plants, there is comparatively very little information available on their biosynthesis and regulation. It is generally believed that the biosynthetic pathway is similar to that of the mammalian system. 3-Hydroxy-3-methyl-glutaryl coenzyme A (HMG-CoA) reductase plays a key role in the regulation of cholesterol biosynthesis in animals, but its role in the regulation of isoprenoid biosynthesis in plants is not yet known. Plant tissues are rich in phenolic compounds and the activity of mevalonate pyrophosphate (MVAPP) decarboxylase in animals is inhibited by phenolic acids. Therefore, it is of interest to see whether other points of regulation besides HMGCoA reductase exist in plant tissues, particularly at the level of MVAPP decarboxylase. In order to verify this point and also to elucidate the role of the mevalonate metabolizing enzymes in the channelling of carbon flow to specific end products, attempts were made to detect the activities of the enzymes involved in the metabolism of mevalonate and to characterize them. Based on the nature of their storage products, four types of plants were selected: (1) protein-bearing (or storing) represented by *Vigna radiata, Vigna catjang and Pisum sativum*; (2) starch-bearing – *Oryza sativa*; (3) oil-bearing – *Arachis hypogaea*; and (4) isoprenoid-bearing – *Ficus elastica* and *Cymbopogon citratus*.

2. Materials and methods

Lemon grass was grown in pots in the Institute nursery and seedlings of mung bean, rice, peas and groundnut were grown in trays on sterilized sand. The plant tissue was homogenized and the microsomal and cytosolic fractions were prepared by differential centrifugation[1]. The assay of HMGCoA reductase was carried out by the method of Shapiro *et al*[2], while the enzymes, mevalonate kinase (MVA), mevalonate phosphokinase (MVAP kinase) and MVAPP decarboxylase were assayed

by the method of Shama Bhat and Ramasarma[3]. For incorporation studies using ^{14}C-acetate the green leaves or seedlings were incubated in phosphate buffer containing ^{14}C-acetate and at the end of the required time period the plant tissue was washed and extracted with methanol in the cold. Lipids were extracted and an aliquot of the lipid fraction was subjected to saponification. The non-saponifiable lipids were fractionated further on an alumina column[4].

3. Results and conclusions

Initially, various plants were screened for their ability to decarboxylate mevalonate and this activity, measured as the release of $^{14}CO_2$ from [1-^{14}C] MVA, was found in all the plants tested. Lemon grass, a plant rich in essential oils, did not show a higher activity compared to that of other plants and therefore it appears that the MVA-metabolizing enzymes do not show any enrichment characteristic of directing or channelling the carbon flow towards the specific end-product (isoprenoid compounds) in these plants tested.

Lemon grass (*Cymbopogon citratus* stapf) was selected for further studies since it contains 10% bydry weight, isoprenoid products and leaf tissue had been studied the least. The activities of the three enzymes, MVA kinase, MVAP kinase and MVAPP decarboxylase were detected in green leaves of lemon grass and their properties were studied. Of the three enzymes, the last one, namely, MVAPP-decarboxylase is being reported for the first time from green leaves of plants. Just as in the case of the rat liver system, MVAPP decarboxylase was the slowest step of the three enzymes (Table I) and the enzyme activity was inhibited by phenolic compounds. A unique feature of MVAPP decarboxylase from lemon grass is that it exhibits seasonal variation with maximum activity being detected in the hot summer months (fig. 1).

Although the activation of the MVA-metabolizing enzymes could be identified in green leaves of lemon grass all attempts made to detect the activity of HMGCoA reductase were unsuccessful. Therefore, further studies were carried out with *Arachis hypogaea*. The activities of HMGCoA reductase, MVA kinase, MVAP kinase and MVAPP decarboxylase were detected in green seedlings of *Arachis hypogaea* and the properties studied (Table II). Unlike the rat liver system, MVAPP decarboxylase appears to be the rate-limiting step in green seedlings of *Arachis hypogaea* and not HMGCoA reductase. The activity of this enzyme is regulated by light and abscisic acid. Treatment of the seedlings with abscisic acid caused a decrease in the activity of MVAPP decarboxylase. The activities of the three MVA-metabolizing enzymes are low in etiolated seedlings compared to controls. These results suggest that in groundnut seedlings regulation of isoprene pathway may operate at the level of mevalonate metabolism.

Table I
Mevalonate metabolism in *Cymbopogon citratus*

Sl no	Test system	Measurement	n moles/h per mg protein
1.	[1-^{14}C]-MVA→$^{14}CO_2$	All three enzymes	11
2.	[1-^{14}C]-MVA→[1-^{14}C]-MVA-P	MVA kinase	473
3.	[1-^{14}C]-MVA-P→[1-^{14}C]-MVA-PP	MVA-P kinase	367
4.	[1-^{14}C]-MVA-PP→$^{14}CO_2$	MVA-PP decarboxylase	45

The plant tissue was homogenized and the enzymes assayed as described in the Materials and Methods.

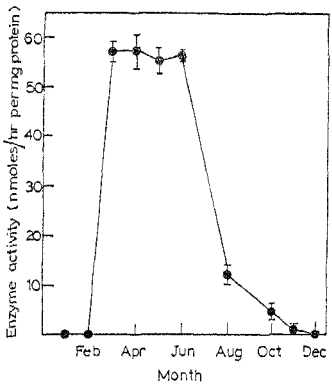

FIG. 1. Seasonal variation in the activity of MVAPP decarboxylase.
The enzyme activity was assayed by the method of Shama Bhat and Ramasarma[3]. The values given are means ±S.D. of independent analysis of three sets in each month.

Table II
Effect of light and treatment with abscisic acid on the activities of HMGCoA reductase, MVA kinase, MVAP kinase and MVAPP decarboxylase in seedlings of *Arachis hypogaea*

Enzyme	Treatment	nmole/h per mg protein	
		Light	Dark
HMGCoA reductase	Control	14.0±0.8	18.9±2.5
	+ABA	13.4±0.31	20.2±3.8
MVA kinase	Control	478±5	118±15
	+ABA	606±16	304±19
MVAP kinase	Control	178±2	48±2
	+ABA	188±36	131±3
MVAPP decarboxylase	Control	3.98±0.30	0.76±0.07
	+ABA	2.40±0.36	1.08±0.12

The seedlings were treated with abscisic acid for 3 h and then the tissue was homogenized and the enzymes assayed.

References

1. LALITHA, R., GEORGE R. AND RAMASARMA, T. Mevalonate decarboxylation in lemon grass leaves, *Phytochemistry*, 1985, **24**, 2569–2571.

2. SHAPIRO, D. J., IMBLUM, R. L AND RODWELL, V. W. Thin-layer chromatographic assay for HMGCoA reductase and mevalonic acid, *Anal. Biochem.*, 1969, **31**, 383–390

3. SHAMA BHAT, C AND RAMASARMA, T. Inhibition of rat liver mevalonate pyrophosphate decarboxylase and mevalonate phosphate kinase by phenyl and phenolic compounds. *Biochem. J.*, 1979, **181**, 143–151.

4. GRIFFITHS, W. T., WALLWORK, J. C AND PENNOCK, J. F. Presence of series of plastoquinones in plants. *Nature*, 1966, **211**, 1037–1039.

Thesis Abstract (Ph.D.)

***Luffa acutangula* agglutinin, a chito-oligosaccharide-specific lectin from the ridge gourd phloem exudate: physicochemical studies** by Vellareddy Anantharam.
Research supervisor: A. Surolia.
Department: Molecular Biophysics Unit.

1. Introduction

Lectins are cell agglutinating and carbohydrate-binding proteins of plant and animal origin[1]. Despite the increasing use of lectins in immunology, cell biology and in the characterization of cell-surface glycoconjugates, many basic biochemical properties of most lectins remain obscure. Concanavalin A, wheat-germ agglutinin, soybean agglutinin and peanut agglutinin are a few exceptions.

Since lectins were initially discovered in plant seeds which are rich sources of these proteins, seed lectins have been most widely studied. However, lectins have also been discovered in other parts of the plants such as stem, leaves, barks and fruits. A detailed analysis of lectins from sources, other than seeds is lacking. Recently, lectins have also been found in the phloem exudates of several members of cucurbitaceae family[2]. Elucidation of their molecular properties in detail should facilitate understanding of structure-function relationship among this class of lectins. This study is a step in that direction[3,4].

2. Results and discussion

The lectin *Luffa acutangula* agglutinin (LAA) has been purified by a combination of ammonium sulfate fractionation and affinity chromatography on soybean agglutinin glycopeptide coupled to Sepharose 6B. The affinity-purified lectin was found homogeneous by polyacrylamide gel electrophoresis in acid and alkaline pH as well as in the presence of sodium dodecyl sulfate (SDS), by analytical gel chromatography, by sedimentation velocity and equilibrium experiments. The molecular weight (M_r) of the native proteins is 48,000 as determined by gel chromatography and sedimentation equilibrium experiments. Subunit molecular weight (M_r) was determined to be 24,000. The subunits are not held together by disulfide bonds as the molecular size did not vary in the presence of 2-mercaptoethanol. The lectin is not a glycoprotein and secondary structure analysis by far UV-CD showed 31% α-helix and rest random coil.

LAA did not show any specificity towards any of the human blood groups A, B and O. Hemagglutination inhibition studies revealed that LAA is absolutely specific for $\beta(1\rightarrow4)$-linked oligomers of N-acetylglucosamine and is not inhibited by any of the monosaccharides tested. The lectin also binds to AsN-linked glycopeptides from soybean agglutinin (high mannose type), ovalbumin (hybrid type) and fetuin (complex type). All these three types of glycopeptides were equally effective

in inhibiting the hemagglutination reaction caused by this lectin. Lack of inhibition by soybean agglutinin oligosaccharide (derived from endo-β-N-acetyl glucosaminidase H treatment of soybean agglutinin glycopeptide) suggests that it is the core chitobiosyl sequences in these glycopeptides which are recognized by the lectin. LAA has two binding sites for saccharides (one per monomer) as determined by equilibrium dialysis experiments and the linearity of the Scatchard Plot at low- and high-saturation ranges, suggesting independence of these two sites and lack of additional sites.

Thermodynamic studies on the carbohydrate-binding properties of LAA, using circular dichroism, UV-difference spectroscopy and fluorescence spectroscopy were performed. Upon addition of chito-oligosaccharides to LAA, there was ligand concentration and size-dependent enhancement in the mean-residue ellipticities in the near UV-CD region (250–300 nm) with a maximum at 280 nm. The association constants (K_a) obtained for the binding of chito-oligosaccharides to LAA increased with increase in chain length up to penta-N-acetylchitopentaose. The values of K_a for di-, tri-, tetra-, penta- and hexa-saccharides of $\beta(\rightarrow 4)$-linked GlcNAc oligomers at 25°C are $0.8 \times 10^3\ M^{-1}$, 8×10^3, 7.2×10^4, 5.25×10^5 and $5.3 \times 10^5\ M^{-1}$, respectively. Thermodynamic parameters obtained from the temperature dependence of K_a values for the binding of saccharide to the lectin show an increase in enthalpy with increase in saccharide chain length up to a tetramer. From these studies it has been proposed that the combining site of LAA is extended, consisting of at least four subsites A, B, C and D.

The mean-residue ellipticity of LAA upon binding to chito-oligosaccharides is enhanced. This increase has been attributed to the perturbation of one or more tryptophan residues in the combining region of the protein. The UV-difference spectra of LAA upon binding to $(GlcNAc)_3$ gave two characteristic maxima at 288 and 292 nm, respectively, further confirming the possible location of tryptophan residue(s) at or near the combining region.

Fluorescence spectrum of LAA shows an emission maximum at 336 nm when excited at 295 nm, which is characteristic of tryptophan emission in proteins. There was a ligand concentration and size-dependent enhancement in the intrinsic fluorescence of the protein. Upon binding to chito-oligosaccharides there was an observable blue shift. A blue shift of 2 and 4 nm was observed for the binding of tri- and tetrasaccharides (as well as pentasaccharide, respectively), whereas the percentage fluorescence increased from 5 to 32 on going from di- to hexasaccharide.

The values of K_a and thermodynamic parameters obtained for the binding of chito-oligosaccharides to LAA correlated well with those obtained by near UV-CD studies. Based on blue shift and percentage fluorescence enhancement a tryptophan residue is presumed to be located in close proximity to the subsite D. The value of K_a, $-\Delta G$, $-\Delta H$ and $-\Delta S$ obtained for the binding of soybean agglutinin glycopeptide to LAA at 23°C are $2.29 \times 10^5\ M^{-1}$, 30.4 kJ mol^{-1}, 32.5 kJ mol^{-1} and 7.1 $mol^{-1}\ K^{-1}$, respectively. An enhancement of 16% in the fluorescence intensity and a blue shift of 2 nm in the emission maximum were also observed upon binding of this glycopeptide to LAA. Soybean agglutinin oligosaccharide and AsN-GlcNAc (derived from endo-β-N-acetylglucosaminidase H treatment of soybean agglutinin glycopeptide) did not have any influence on the intrinsic fluorescence of LAA. From these data it can be interpreted that the binding of chito-oligosaccharides to LAA up to the tetramer is enthalpically driven whereas the better binding of soybean agglutinin glycopeptide is entropically favoured.

Dynamic quenching studies with acrylamide and succinimide gave a ratio of $K_S/K_A = 0.6$ (where K_S and K_A are the quenching constants for succinimide and acrylamide, respectively) suggesting that the tryptophan residues are located at regions on the protein highly accessible to the solvent. A decrease in the quenching constant for iodide ion in the presence of tetra-N-acetylchitotetraose suggests that some of the tryptophan residues are being shielded from the quencher by the bound ligand. This indicates the involvement of tryptophan residues in the biological activity of LAA.

Modification of tryptophan residues alone led to a complete loss in both the hemagglutinating and carbohydrate-binding activities. Under denaturing conditions, six residues/molecule were available for modification, whereas only two residues/molecule were available under native conditions. The relative loss in the hemagglutinating activity, after modification, revealed that two tryptophan residues/molecule are required for lectin activity. These results were further substantiated by protection experiments, where it was observed that chito-oligosaccharides protected the active-site tryptophan residue from modification in LAA.

References

1. SHARON, N. AND LIS, H. — *Annu. Rev. Biochem.*, 1986, **55**, 35–67.
2. ALLEN, A. K. — *Biochem. J.*, 1979, **183**, 133–137.
3. ANANTHARAM, V., PATANJALI, S. R. AND SUROLIA, A. — *J. Biosci.*, 1985, **8**, 403.
4. ANANTHARAM, V., PATANJALI, S. R. SWAMY, M. J., SANADI, A. R., GOLDSTEIN, I. J. AND SUROLIA, A. — *J. Biol. Chem.*, 1986, **261**, 14621–14627.

Thesis Abstract (Ph.D.)

Membrane channel-forming polypeptides. Studies on alamethiein, antiamoebin and related peptides by Manoj Kumar Das.
Research supervisor: P. Balaram.
Department: Molecuar Biophysics Unit.

1. Introduction

Membrane channel-forming polypeptides possessing ionophoric activity have been widely investigated as models for transmembrane ion transport and for their effects on both artificial and natural membranes. In this study, alamethicin, antiamoebin and other related peptides have been taken up for investigation of their effects on mitochondria and liposomes. A detailed conformational analysis of antiamoebin has been carried out using NMR spectroscopy. The ionophoric properties of antiamoebin and several other synthetic peptides have also been studied.

2. Experimental procedures

Small unilamellar liposomes were prepared by procedures described earlier[1]. Mitochondria were isolated from rat liver and peptide effects on the respiration of mitochondria were monitored using an oxygen-consumption assay as described earlier[2].

The conformational studies on antiamoebin were carried out using 270 MHz ^{1}H and 67.89 MHz ^{13}C NMR. The ionophoric activity of the various peptides were examined by comparing their ability to promote Ca^{2+} fluxes into liposomes and uncoupling oxidative phosphorylation in mitochondria according to the procedures described earlier[3].

The peptides, alamethicin and antiamoebin, were kind gifts from Drs Joseph E. Grady and Richard L. Keene of Upjohn Company, Kalamazoo, Michigan and Dr N. Narasimhachari, Medical College

of Virginia, Virginia Commonwealth University. Melittin was purchased from Sigma Chemical Company, USA. Tetraacetyl and tetrasuccinyl melittin were prepared using published procedures[4]. The other peptides namely, the emerimicin fragments, the Zervamicin fragments and the $(Aib\text{-}Val)_n$ model peptides were synthesized in the laboratory.

3. Main results and conclusions

Studies on the effects of alamethicin on rat liver mitochondria show that the peptide acts as a typical uncoupler at low phosphate (Pi) concentrations (2.5 to 25 mM) but as an inhibitor at high concentrations (50 to 100 mM). No disruption of mitochondrial integrity has been observed by electron microscopy even at the highest concentrations of the peptide used in this assay. This is in contrast to gramicidin, a well-studied channel and uncoupler[5,6], which acts as an uncoupler irrespective of the Pi concentration in the medium. Identical transition from uncoupling to inhibition is observed in the case of tetraacetyl melittin. With melittin, the inhibition at high Pi is not as pronounced. Tetrasuccinyl melittin shows no uncoupling activity (fig. 1).

Investigations into the electron transport chain showed complex IV (cytochrome oxidase) to be the main site of peptide-induced inhibition at high Pi. The observed effects have been interpreted in terms of the differences in Pi transport across the mitochondrial membrane mediated by peptide channels. An increase in the intramitochondrial Pi concentration could result in the inhibition of the binding of cytochrome C to cytochrome oxidase.

Antiamoebin, a microheterogeneous fungal polypeptide rich in α-aminoiso-butyric acid (Aib)[7] has been studied for its membrane-modifying properties. Natural antiamoebin has been fractionated into four components by reverse-phase HPLC. All four fractions have been shown to be effective as Ca^{2+} translocators and mitochondrial uncouplers. In contrast to alamethicin, antiamoebin does not show a Pi-dependent transition from uncoupling to inhibitory activity in mitochondria.

The conformation of natural antiamoebin has been studied using one- and two-dimensional NMR techniques, in dimethyl sulfoxide solutions. Both 270 MHz ^1H and 67.89 HMz ^{13}C-NMR spectra are found to be fully consistent with the amino-acid composition of antiamoebin I. Assignment of a large number of resonances has been achieved by two-dimensional correlated spectroscopy (COSY) and observation of nuclear overhauser effects (NOEs) between various protons. The NMR results have led to the formulation of an intramolecular hydrogen-bonding scheme and subsequently to the generation of two stereochemically acceptable conformations (fig. 2). The two conformations are distinctly different in overall appearance, with one of them assuming an elongated helical structure particularly suitable for functioning as a membrane-spanning helical polypeptide.

Several synthetic, neutral, and α-amino isobutyric acid (Aib)-containing peptides have been studied for their membrane-modifying activity using the assays of Ca^{2+} flux into liposomes and uncoupling of oxidative phosphorylation in mitochondria. The peptides studied include emerimicin fragments ranging in length from 5 to 11 residues, model $(Aib\text{-}Val)_n$ sequences ranging in size from 5 to 10 residues and the 10- and 16-residue peptides corresponding to the sequence of an apolar Zervamicin II A analog.

In the case of emerimicin fragments, mitochondrial uncoupling activity increases with chain length for the 7-, 8-, 9- and 11-residue peptides. The 10-residue amino-terminal fragment behaved anomalously exhibiting much lower activity. This observation may be linked to the presence of a C-terminal Hyp residue in this peptide. All the peptides failed to facilitate Ca^{2+} translocation across lipid bilayers.

Interestingly, for the synthetic fragments of Zervamicin, a 10-residue peptide, Boc-Trp-Ile-Ala-Aib-

Ile-Val-Aib-Leu-Aib-Pro-OMe (ZA1-10) is found to show greater activity than a 16-residue peptide, Boc-Trp-Ile-Ala-Aib-Ile-Val-Aib-Leu-Aib-Pro-Ala-Aib-Pro-Aib-Pro-Phe-OMe (ZA1-16). Among the model oligopeptides with $(Aib\text{-}X)_n$ alternate sequences, only the 10-residue peptide, $Boc\text{-}(Aib\text{-}Val)_5\text{-}OMe$ (V_{10}) showed Ca^{2+} transport activity. Its mitochondrial uncoupling activity was found to be higher than the 7-residue peptide. Comparison of this peptide with other 10-residue peptides, $Boc\text{-}Phe\text{-}(Aib)_3\text{-}Val\text{-}Gly\text{-}Leu\text{-}Aib\text{-}Aib\text{-}Hpy\text{-}OMe$ (E_{10}) and ZA1-10, showed that the efficiency of Ca^{2+} transport by these peptides followed the order, $V_{10} > ZA1\text{-}10 > E_{10}$. A similar comparison of

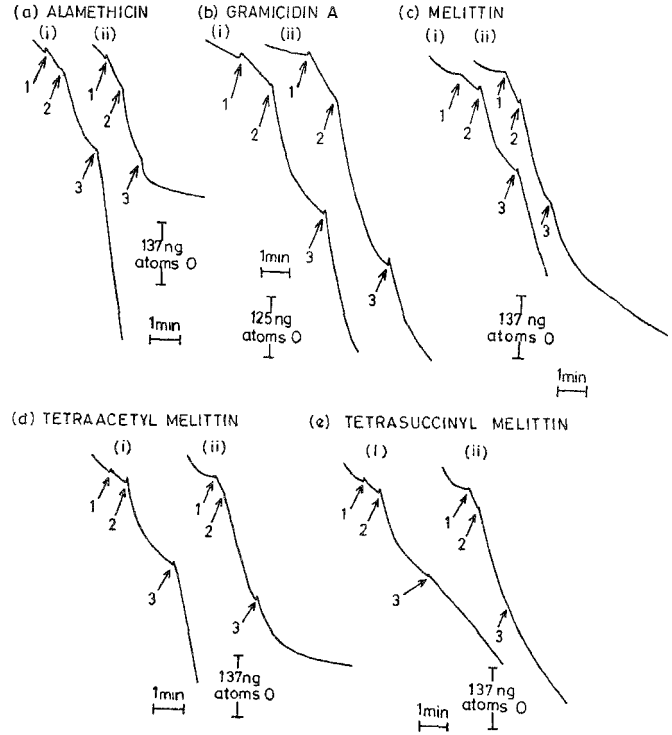

FIG. 1. A comparison of the effects of (a) alamethicin, (b) gramicidin, (c) melittin, (d) tetraacetyl melittin, (e) tetrasuccinyl melittin on state 4 respiration of rat liver mitochondria suspended in media containing (i) 2.5 mM Pi and (ii) 100 mM Pi. Peptide concentration $\sim 3\,\mu M$; mitochondrial protein concentration $\sim 0.5\,mg\,ml^{-1}$. Arrows 1, 2 and 3 indicate points of addition of succinate (7.5 mM), ADP (72μM for a, c, d, e or 130μM for b) and peptide, respectively.

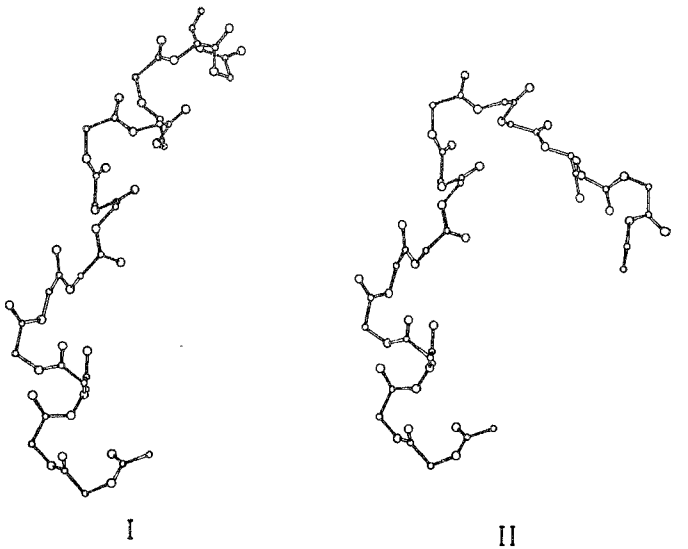

FIG. 2 Perspective view of suggested backbone conformations I and II of antiamoebin consistent with the NMR data and stereo-chemical constraints.

V_{10} with the longer peptides, antiamoebin (16 residues) and ZA(1–16) (16 residues) has shown the order of uncoupling activity as antiamoebin > $V_{10} \gg$ ZA1-16.

The results obtained show that there does not appear to be a uniform correlation between chain length and membrane-modifying activity for all classes of peptides studied. Further, a direct correlation between the two assay systems used is not obtained for all classes of peptides, suggesting thereby that the structural characteristics of the pores necessary for mitochondrial uncoupling and Ca^{2+} flux may be quite different.

References

1. BARENHOLZ, Y., GIBBES, D., LITMAN, B. J., GOLL, J., THOMPSON, T. E. AND CARLSON, F. D. *Biochemistry*, 1977, **16**, 2806–2810.

2. DAS, M. K. AND BALARAM, P. *J. Biosci.*, 1984, **6**, 337–348.

3. MATHEW, M. K., NAGARAJ, R. AND BALARAM, P. *J. Membrane Biol.*, 1982, **65**, 13–17.

4. HABERMANN, E. AND KOWALLEK, H. *Hoppe-Seyler's Z. Physiol. Chem.*, 1970, **351**, 884–890.

5. WALLACE, B. A. *Biophys. J.*, 1986, **49**, 295–306.

6. CHAPPELL, J. B. AND CROFTS, A. R. *Biochem. J.*, 1965, **95**, 393–402.

7. PANDEY, R. C., MENG, H., CARTER COOK, J. JR. AND RINEHART, K. L. JR. *J. Am. Chem. Soc.*, 1977, **99**, 5203–5205.

Thesis Abstract (Ph.D.)

Pressure as a parameter in the study of electrical and defect behaviour of metals and alloys

by Mohammad Yousuf.
Research supervisors: E. S. Raja Gopal and K. Govinda Rajan (Materials Science Laboratory, Indira Gandhi Centre, Kalpakkam).
Department: Physics.

1. Introduction

This communication is directed to elucidate the role of high pressure in the study of solids. The examples are somewhat selective in nature. For example, electrical resistivity of nickel and iron is investigated as a function of pressure and temperature. Owing to the fact that these above transition metals are itinerent ferromagnets, an interplay between the electronic and magnetic degrees of freedom is possible[1]. Defect solid state is another area where the role of pressure is brought in as a thermodynamic parameter to delineate the operating mechanisms during the recovery or relaxation. This is exemplified by considering the cases of cold-deformed stainless steel, thorium, uraniam and metallic glass[2,3].

2. Experimental programme

An opposed anvil high-pressure device (OAHPD) has been developed to carry out high-pressure experiment. Electrical resistivity is the measuring tool. The OAHPD has been extended to incorporate the high temperature also. While pressure capability of OAHPD is ~ 100 kbar, an *in situ* temperature of $\sim 1300°C$ can be generated. The electrical resistivity could be measured to a resolution of 1 in 10^6 and the quantity $\partial/n\rho/\partial p$ to 1 in 5×10^5.

High-pressure and temperature electrical resistivity of nickel and iron is shown in fig. 1. dT_C/dP of nickel and iron are $+0.41$ K kbar^{-1} and ± 0.02 K kbar^{-1}, respectively. What is more interesting is the way in which pressure affects the resistivity of nickel below and above T_C. For instance, at $T < T_C$, ρ decreases with pressure and the PCR is -1.6×10^{-3} K kbar. However, at $T > T_C$, ρ increases with pressure and the PCR is $+8.5 \times 10^{-4}$ K kbar. Thus, there is a change of sign in the PCR across the magnetic transition. Similar experiments on iron, on the other hand, reveal no such anomalous behaviour.

For a pure ferromagnetic transition metal,

$$\rho = \rho_{s-d} + \rho_{mag} + \rho_{es,ed} \tag{1}$$

where

$$\rho_{s-d} = \frac{3k_B}{\hbar c^2} V \frac{N^{\uparrow}(E_F) + N^{\downarrow}(E_F)\{\lambda_{tr}/\langle v^2 \rangle_s}{N^{\uparrow}(E_F)N^{\downarrow}(E_F)} \frac{\lambda_{tr}}{\langle v^2 \rangle_s} \tag{2}$$

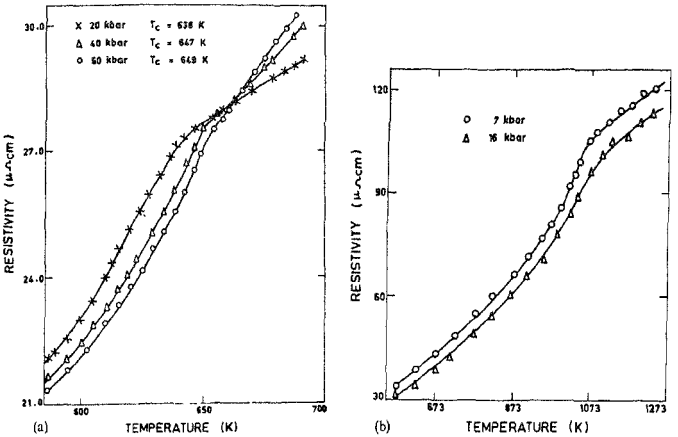

FIG. 1. High-pressure and temperature electrical resistivity of nickel and iron. The change of slope occurs at the magnetic transition temperature, T_C. The reversal in the behaviour of resistivity of nickel as a function of pressure can be seen at temperature above T_C.

$$\rho_{mag} = \frac{\pi\hbar|p|^2}{6e^2m^2(v_F^2)}\langle(\hat{\nabla}\cdot\hat{M})^2\rangle\frac{N_s^\uparrow N_d^\downarrow + N_s^\downarrow N_d^\uparrow}{(N_s^\uparrow + N_d^\downarrow)} \tag{3}$$

and

$$\rho_{es,ed} = 8.1\times10^{19}\frac{\pi^4e^2}{16}\frac{1}{v_sE_F}\frac{k_F}{q}\left(\frac{v_s-1}{v_d}\right)^2\left(\frac{k_BT}{E_F}\right)^2. \tag{4}$$

Here $N(E_F)$, λ_{tr}, V and $\langle v^2\rangle_s$ are the total electron density of states at the Fermi level, the electron mass enhancement factor, the atomic volume and the expectation value of the square of the Fermi velocity, respectively, $|p|$ is the momentum transfer during electron-magnon scattering, $\langle(\underline{v}\cdot\hat{M})\rangle^2$ refers to the spatial variation in $\hat{M}$ (the unit vector in the direction of local magnetisation) and m is the mass of the electron. v_s, v_d and E_F are the velocities of sp- and d-electrons and the Fermi energy, respectively. Using the values of various parameters of nickel, eqn (1) can be written as:

$$\rho(\mu\Omega\text{cm}) = 6.972\times10^{-3}T + 20.654\left(\frac{T}{T_C}\right)^2 + 9.362\times10^{-6}T^2. \tag{5}$$

Using eqn (5), ρ is calculated as a function of temperature which gives a good agreement with the data points. Incorporating the pressure dependence of various factors in eqns (2–4), electrical resistivity as a function of pressure and temperature is calculated which indicates a discrepancy with the data points above 650 K. Thus, since the expression for resistivity of nickel does not reproduce even qualitatively the observed behaviour above T_C, it is clear that a significant feature must be missing from it. Mott's conjecture provides an elegant solution to this discrepancy. As a consequence of the FS change at T_C, the spin-spin coupling becomes weaker in the paramagnetic phase rendering spin-flip

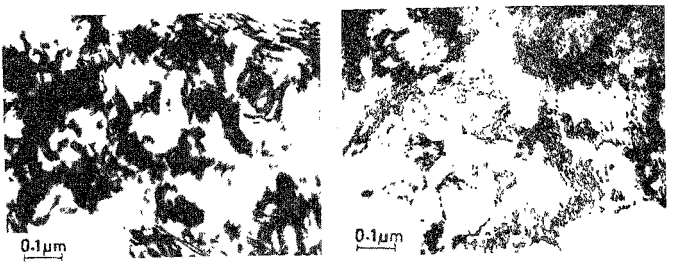

(a) (b)

FIG. 2. (a) Microstructure of cold-worked stainless steel, (b) Dislocation structure transforms to a sub-granular structure after a pressure treatment above 20 kbar.

possible during the electron-electron scattering. This process is an exchange version of the Baber mechanism in which the momentum is conserved, while the current is not. Since the probability of scattering is found to vary as the square of the exchange overlap, and since under compression the exchange overlap increases, it is expected that the probability of electron-electron scattering increases with pressure. Thus, the resistivity should show an increase with pressure. In iron, we note that the spin-spin coupling is quite strong even in the paramagnetic phase and hence the exchange version of the Baber mechanism is not the dominant factor.

Turning now to the analysis of the data of nickel near the critical region, it is noted that the magnetic energy and the spin-dependent resistivity have the same form. The least-square fitting of the data in the critical region leads to pressure-independent (universal) amplitude ration and leading exponents, as expected from the R.G. theory[4]. Their values are $\alpha = \alpha' = -0.1083 \pm 0.0004$, $A/A' = 1.124 \pm 0.002$ and $D/D' = 1.15 \pm 0.02$.

The experiment on severely cold-deformed stainless steel indicates a minimum in the reduced resistivity ratio at 20 kbar with a characteristic relaxation time of 500 s. Transmission electron microscopy reveals that samples pressure-treated above 20 kbar have a sub-granular dislocation structure[3] (fig. 2). Hydrostatic pressure measurements performed on the amorphous alloy Fe_{40} Ni_{40} $P_{14}B_6$ reveal that the two prominent structural relaxation stages occurring at 240 and 350°C can be brought to room temperature by the application of 40 and 60 kbar, respectively, as indicated by the resistivity and X-ray diffraction studies[3].

References

1. MOHAMMAD YOUSUF, SAHU, P. CH. AND GOVINDA RAJAN, K. — High pressure and high temperature electrical resistivity of ferromagnetic transition metals: nickel and iron, *Phys. Rev B· Condensed Matter* (under print).

2. MOHAMMAD YOUSUF, SAHU, P. CH., RAGHUNATHAN, V. S. AND GOVINDA RAJAN, K. — Recovery in cold-worked alloy under pressure: example of AISI 316 stainless steel, *J. Mater Sci.*, 1986, **211**, 1956–1962.

3. MOHAMMAD YOUSUF AND GOVINDA RAJAN, K. — Pressure induced structural relaxation in amorphous solids-example of Fe_{40} $Ni_{40}P_{14}B_6$, *J. Mater. Sci. Lett.*, 1984, 3, 149–152.